INDONESIAN JOURNAL ON GEOSCIENCE
Geological Agency
Ministry of Energy and Mineral Resources

Journal homepage: http://ijog.geologi.esdm.go.id
ISSN 2355-9314, e-ISSN 2355-9306

Spatial Simulation Model of Bauxite Grades Using R Data Analysis: Its Implication for Exploration Activity

[1]Rosmalia Dita Nugraheni, [2]Dedi Sunjaya, [2]Bronto Sutopo, [1]Mohammad Apriniyadi, [1]Cahyaningratri Prima Riyandhani, and [1]Imam Setiaji Ronoatmojo

[1]Department of Geological Engineering, Faculty of Earth Technology and Energy, Universitas Trisakti, Jakarta, Indonesia
[2]P.T. ANTAM, Tbk. Jln. Letjen. T.B. Simatupang No.1, Lingkar Selatan, Tanjung Barat, Jakarta, Indonesia

Corresponding author: rosmalia.dn@trisakti.ac.id
Manuscript received: March, 12, 2021; revised: November, 1, 2021;
approved: May, 14, 2022; available online: October, 3, 2022

Abstract - In exploration, the investigation of prospective area encounters several barriers of land ownership, budget limitation, and exhausting permit procedures. To speed up the exploration activities of bauxite deposits and bauxite characteristics, grades of the gap areas should be simulated based on the available test pit data sets. This study aims to address the limitations and to optimize the exploration boundaries using the R project for statistical computation. R data analysis weaves the framework of kriging that required information from the adjacent data. This study utilizes the geochemical data of Al_2O_3, Fe_2O_3, SiO_2, and TiO_2 from 296 test pit sampling points. The geochemical data used for R analysis were taken from bauxite horizon, while the other mineralogical properties were taken entirely from the exposed bedrock and test pit data. To verify the result of R analysis, recent data of the simulated area were used as a comparison. The R result shows the prediction value is slightly below the actual value of Al_2O_3. The kriging simulation of Al_2O_3 was correlated with test pit and mineralogical characteristics of samples. This reveals the predicted value of simulation closely represents the true value of Al_2O_3 grades. Extrapolation results of Fe_2O_3 and $RSiO_2$ with regards to Al_2O_3 grades suggest that higher grade of bauxite underwent desilication and deferruginization as evidenced by a high value of Index of Lateritization. It can be inferred that this attempt points out the advantages of a quick and reliable projection of bauxite laterite deposits from the limited parameters

Keywords: kriging estimation, simulation, bauxite laterite, Index of Lateritization, desilication, deferruginization

How to cite this article:
Nugraheni, R.D., Sunjaya, D.,Sutopo, B., Apriniyadi, M., Riyandhani, C.P., and Ronoatmojo, I.S., 2022. Spatial Simulation Model of Bauxite Grades Using R Data Analysis: Its Implication for Exploration Activity. *Indonesian Journal on Geoscience*, 9 (3), p.337-353. DOI: 10.17014/ijog.9.3.337-353

Introduction

Background

Lateritic bauxite deposits have a significant input to fulfil the global demand for aluminium. The deposits are derived from complex interactions between aluminosilicate rocks and local physiochemical weathering environments. The external weathering variables, such as climate, geomorphology, tectonic setting, pH-Eh conditions, and hydrologic conditions (Hedenquist *et al.*, 2019) diversify the characteristics of bauxite in the area of exploration in Tayan District, Sanggau, West Kalimantan Province. It ultimately requires test pit examination to acquire the vertical profile of bauxite characteristics. However, the investigation somehow has some constraints, such as the status of land owner-

ship, budget restriction, and exhausting permit procedures.

In the meantime, exploration activities present as a prominent step to identify the prospective areas of mining. In bauxite exploration, this activity involves continuous stages of geological mapping, test pitting, grid, and GPS measurement as well as rock sampling. The methods need to be carried out perpetually for data assurance by implementing a closer grid measurement in detailed exploration stages. The realization of these stages is different from one place to another, but the prevalent impediment in conducting test pit also comes from local communities that require prerequisite for test pit authorization. To address the issues, while continuing the progressive exploration activities, an attempt of ore grade estimation needs to be carried out as a practical solution using statistical data analysis in terms of R.

R data analysis is used to simulate the incomplete data of orebody boundaries. The R data analysis presents as a statistical computing language which is described as syntaxial language equipped with great features of data visualization (Bivand *et al*., 2008; Kabacoff, 2011). R is specifically designed for data science community that is familiar with the programming environment. This analysis emphasizes the analytic-driven decision in fulfilling the gap data before making extrapolation of geochemical data. The R data analysis was built from conceptual knowledge (Strebelle, 2002) that allows the simulation of spatial functions by reproducing statistical pattern or taking data from nearby sampling point as analogue sites (Oriani *et al*., 2014; Pirot *et al*., 2014). So far, the application of R data analysis in the mining industry is not yet widely used. A geostatistical approach presents a fast parameter for tuning the incomplete data. Therefore, this study attempts to address the gap data and/or reproducing statistical pattern from an exhaustive data set.

Tectonic Settings

The northwest Kalimantan belongs to the Pretertiary continental blocks of the Sundaland Cratons (de Smet and Barber, 2005). The continental blocks were amalgamated with regards to the closing suture of the Paleotethys Ocean in the Late Triassic. The origin of southwest Kalimantan block remains debatable, where some authors believe that this block had been rifted from the NW Australia margin in the Late Jurassic time, and collided with SE Asia in the Mid-Cretaceous time (Hall, 2002; 2018). In contrast, Metcalfe (2011, 2017) argued that the origin of Sundaland amalgamation is in the Late Triassic or as different microplate derived from Indochina. The intense paleo-weathering was recorded that it had taken place during the event of Tethys closure in the Upper Paleozoic to Mesozoic which was accompanied by a collision and an uplift (Putzolu *et al*., 2018). While the most favourable period of bauxitization occurred in the Cretaceous to Eocene time (Herrington *et al*., 2016).

Local Geological Setting

The geological setting of the studied area were collected from the field geological observation towards the exposures of bauxite parent rock. Tracking location was done along the ridge of Segelam. The hill is considered as a multiple-intrusion, produced by subsequent extensional faulting during Late Cretaceous. From older to younger, the rock units are sequentially explained as follows (Figure 1).

Diorite unit is exposed largely in the Segelam ridges, which is situated in the southern part of the Kapuas River. The rock has the characteristics of fresh grey colour to brownish grey colour under weathering condition, holocrystalline, and hypidiomorphic granular. The crystal size is about 1-3 cm, comprising predominant plagioclase with subordinate hornblende, lesser pyroxene, chlorite, sericite-illite, and opaque minerals. Sphene presents as accessory minerals together with zircon. Diorite was observed from the depth of 2.9 m below the soil surface. To the south, diorite is intruded by quartz monzodiorite. Based on the regional geological map, diorite rock unit is equivalent to the Sepauk Tonalite (Kls) of Upper Cretaceous age.

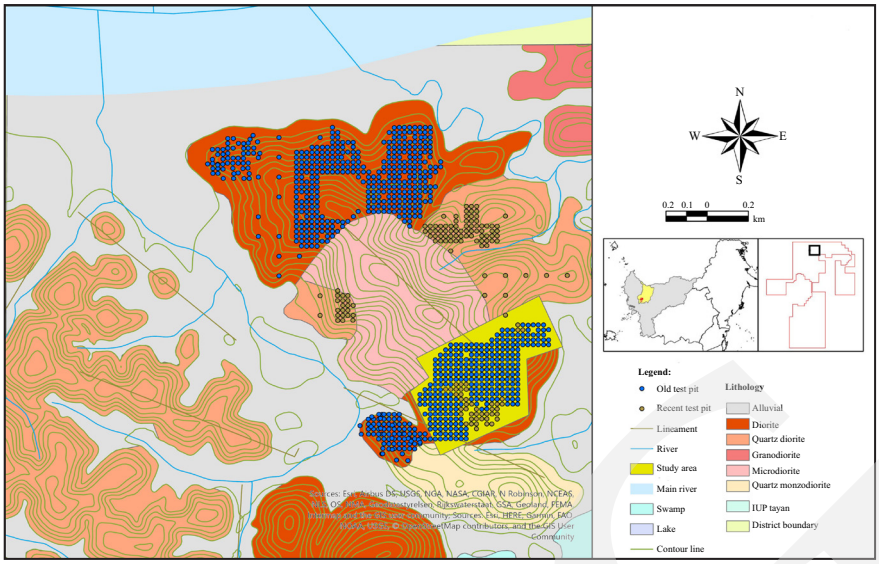

Figure 1. Geological map of Tayan District.

Quartz monzodiorite intrudes the diorite rock unit. The rock unit lies in the southeastern part of Segelam Hill. Well exposed quartz monzodiorite were observed under 4.2 m depth from the top exposure. The rocks exhibit grey to brownish grey, holocrystalline, hypidiomorphic granular, and 2 - 4 mm sized crystals. The lithology is predominated by plagioclase, subordinate quartz with minor orthoclase, hornblende, and biotite. Plagioclase is slightly altered to sericite, suggesting that the rock underwent deuteric alteration. Sphene presents as an accessory mineral.

In contrast, quartz diorite intrudes the diorite rock unit in the middle part of the Segelam Hill. The rock unit denotes the magmatism in the Late Cretaceous, which is equivalent to the Sepauk Tonalite. The lithology exhibits grey to brownish grey colour, equigranular, phaneritic, and holocrystalline. The main mineralogical compositions are plagioclase and quartz with lesser biotite and hornblende.

Microdiorite pyroxene presents as the last intrusion which was intruded by diorite and quartz diorite rock units. Microdiorite pyroxene is the youngest rock unit that is mainly spread in the centre of the Segelam ridge. The rock exhibits greyish black colour, holocrystalline, with 1 - 4 mm sized crystals, subhedral to anhedral, composed of predominant plagioclase and groundmass, subordinate pyroxene, with lesser hornblende, biotite, and opaque minerals.

Alluvium, beach, swamp, and terrace deposits (Qa) are Quaternary deposits that cover most of alluvium plain and river valley of Kapuas. The deposits in the west of Nangataman, along the Kapuas River and the north of Tayan, are characterized by alluvial, tidal lacustrine, swamp, and terrace deposits that present as loose sediments of mud, sand, granule, and plant remains.

Materials and Methods

Methods and Materials

Bauxite samples were collected from 296 test pits during the exploration stage of P.T. Antam Tbk. at Tayan District, Sanggau, West Kalimantan. Test pit points have 25 m spacing with each fixed point were recorded using GPS, and were plotted on the location map using ARC GIS and R. The maximum depth of pitting was performed on the upper part layer of kong/pallid zone. The description for the vertical weathering profile was carried out either from test pits and outcrops. The sampling method was carried out using channel sampling by perforating the wall of the pit. Bauxite grades were recorded every 2 m from the top bauxite horizon. The preparation was

performed for bauxite samples which includes crude washing, crushing, and pulverizing into 200 mesh to obtain homogeneous samples. The powder samples were then coned and quartered for laboratory analysis and as duplicates. The collected bauxite samples were then analyzed for X-Ray Fluorescence (XRF) to obtain the grades of major elements, such as Al_2O_3, Fe_2O_3, $TSiO_2$, and TiO_2. Elemental analysis is carried out using PANalytical wavelength dispersive X-ray fluorescence (WDXRF) spectrometer. The proportion of reactive silica ($RSiO_2$) was performed using classical wet analysis. Geochemical data used in this study is washed bauxite, but beneficiation was performed accordingly referring to the standard procedures.

Geochemical map of each major element in this research utilized geostatistic concepts by applying the relationship of multiple-elements, besides taking into account the compositional properties of the input data. Test pit data were recorded from 2006 to 2019, and mainly collected grades of Al_2O_3, Fe_2O_3, $TSiO_2$, TiO_2, and $RSiO_2$ from bauxite zone. A total of 296 test pit data were performed for simulation using R. The method for simulation introduces the Ordinary Kriging (OK) which was commenced with experimental variogram and curve fitting (Song *et al*., 2019). The output of this method is an extrapolation model of geochemical grades. Major elements were also being plotted to the ternary diagram of SiO_2-Al_2O_3-Fe_2O_3 (after Aleva, 1994) to show the mineralogical classification of the bauxite ores. Ternary plot of SiO_2-Al_2O_3-Fe_2O_3 (after Schellmann, 1986) was used to determine the degree of lateritization of bauxite deposit.

Mineralogical compositions and characteristics for each horizon samples were observed from petrography and X-Ray diffraction (XRD) analysis. Twelve samples were analyzed for petrography including fresh to slightly weathered rocks and bauxite samples. Fresh rocks were mostly taken from the rock exposure since pitting were only performed until the top of pallid zone (kong). These rocks represent the parent rock of bauxite that are rarely exposed in the studied area. For depicting the mineralogical composition of bauxite and pallid zone, nine bauxite samples and seven kong samples were selected for XRD analysis. This analysis was performed using a Phillips analytical X'Pert powder diffractometer at the XRD Laboratory of P.T. ANTAM.

R Simulation

Bauxite grades, which are recorded every 2 m from the top bauxite zone, show decreasing grades of Al_2O_3 due to ionic mobility. Therefore, the grade extrapolation using R was mainly performed for the top bauxite horizon to predict each geochemical compound. Despite utilizing the washed bauxite, all samples were treated accordingly to minimize miss-concept between washed and unwashed, since Indonesian bauxite requires washing treatment which is different to other countries including Australia and Brazil.

Simulation has mainly been performed for the unexplored area, in which it is defined as the area where the grade of alumina will be predicted from the adjacent test pit data. Analysis of random fields have often been applied using geostatistics which involves estimation and modelling of spatial correlation and its refinement. In R analysis, the analysis was deal with Gstat package. Gstat package has the widest function in geostatistics which covers variogram modelling, ordinary kriging, multivariate geostatistics, and many combinations (Bivand *et al*., 2008).

This study applies R data analysis to model the grade distribution of Al_2O_3, Fe_2O_3, $TSiO_2$, and $RSiO_2$. R data analysis utilizes the grades from the first 2 m depth of bauxite horizon. Some of the simulations implement closed grid distance of 10 m. Reconstruction of geochemical data using R was carried out by applying the ordinary kriging (OK). Ordinary kriging presents as an unbiased method used in ore grade interpolation. The OK uses variogram where information was taken between two test pit points to estimate the weight of the samples. The bauxite horizon is distinctly heterogeneous concerning the attribute in a lateral direction**.** To model the heterogeneity of the predicted grades, anisotropic kriging has

also been performed. Afterwards, the predicted value has been validated using statistical cross-validation that has automatically been generated from the R script.

Kriging Estimation and Variance

The ordinary and universal kriging are simulated using R data analysis, where they will be applied based on two-point geostatistics. In the kriging method, it is important to consider the experimental variogram to understand the spatial variability of ore grades. The first step of R analysis is plotting of test pit location (Figure 2a). The distance between test pit points or sample points is about 25 m. This distance automatically becomes the lag distance. The spatial correlation was then illustrated using variogram which plots semivariance as a distance function. The equation for experimental variogram is written in Equation 1 (Song *et al*., 2019). Lag distance has been calculated from the variogram.

$$\gamma(x,h) = \frac{1}{2}E\left[Z(x) - Z(X+h)\right]^2 \quad \text{..... (1)}$$

where γ(x,h) as the variogram value.

By looking at test pit location in Figure 2a, the spatial ore grade estimation would be predicted in the empty areas of southeast and northwest direction. In kriging estimation, Z(x) and Z(x+h) are the ore grade value from recognizable Z test pit variable at positions of x and x+h. Variation of the observed ore grade is depicted as a histogram (Figure 2b), while the spatial variation has been reconstructed from the experimental variogram. This variogram subsequently underwent curve fitting before it was illustrated as theoretical variogram model. This study applies theoretical variogram using a spherical model and considering the nugget, sill, and the range value (Figure 2c). Somehow, the model levels out at a certain distance as it was

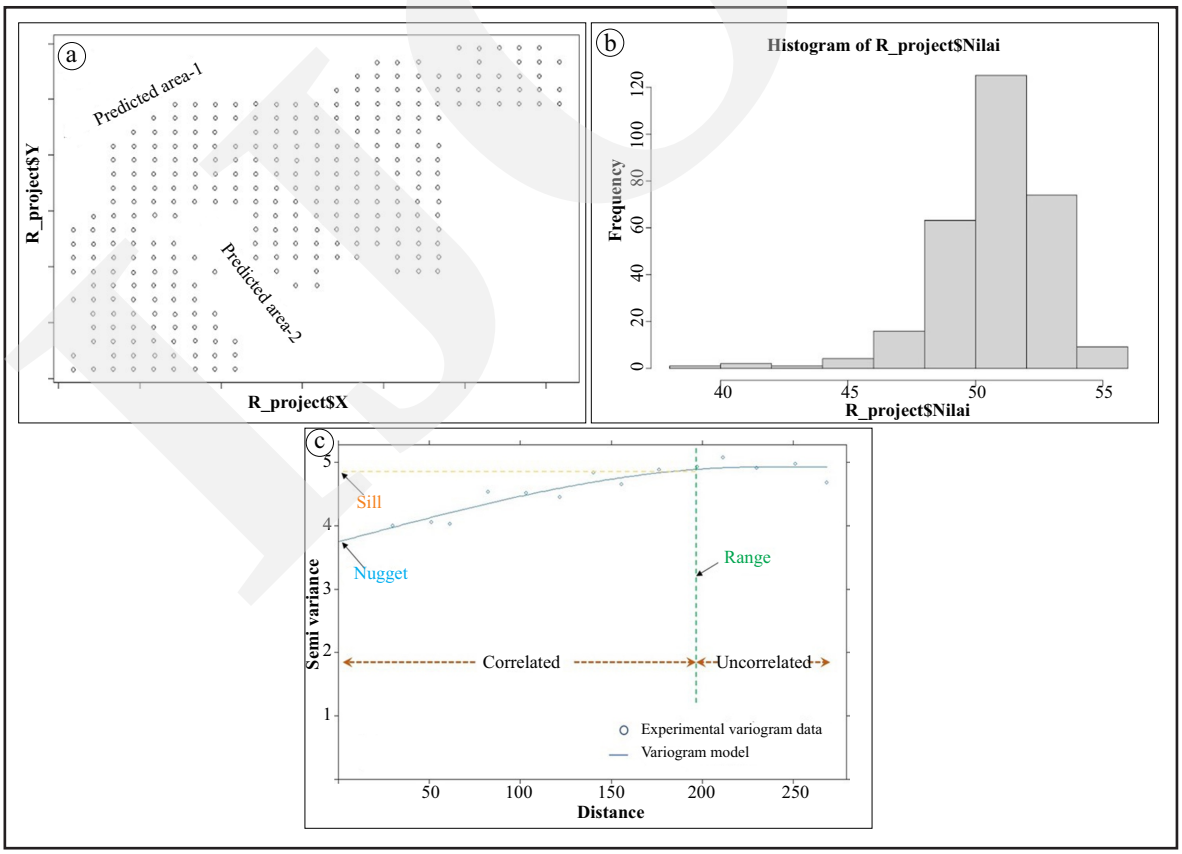

Figure 2. Reconstruction results using R. a) Plot of location map for 25 m grid point, b) Sample grade distribution of Al_2O_3, c) Fitting a variogram model from a lag of experimental variogram.

flattened out. Thus, in semivariogram, the range is spatially autocorrelated. Sill was retracted from the range to the value on the Y-axis, while nugget is attributed to the variation of spatial sources once distances smaller than the interval of sampling. The ore grade of the unknown or blank areas was then estimated using Ordinary Kriging.

Ordinary Kriging (OK)

In OK, the ore grade at a certain grid point can be evaluated using Equation 2, where $Z^*_V(x)$ presents as an estimation value in the estimated grid point, x_i as the most recent sample around the estimated points. $Z(x_i)$ is the grade value of i within the estimated range. The estimation in this equation depends on λ_i as the weight coefficient.

$$Z^*_v(x) = \sum_{i=n}^{n} \lambda i Z(xi) \quad \text{..... (2)}$$

Cross Validation

To measure the degree of bias, cross validation was created by calculating the Mean Error (ME) and Mean Squared Deviation Ratio (MSDR). The ME value should be close to zero, while the MSDR that illustrates the ratio of residuals with kriging variance should have a value close to 1 for the specified model. The ME illustrates the average value of all errors in cross validation. A positive value suggests that the predicted value is larger than the true/ actual value, while a negative value of error indicates that the predicted value is lesser than the true value.

Universal Kriging

Universal Kriging (UK) is carried out by incorporating the local trend of neighbourhood data to provide a smooth variant function of coordinate. This kriging is the extension stages of OK which is taking into account the anisotropy. This consideration was taken as the data set varying differently in a certain direction. The heterogeneity might occur with regards to topography. The studied areas have steep sloping hill; thus, their variogram map (Figure 3a) typically varies in two-directional trends. To simulate the UK by incorporating the anisotropy, new variogram models were displayed for five directions, such as 0°, 45°, 135°, 225°, and 315° illustrated in Figure 3b. Variogram fitting results show that the local trend was in 315° direction. Eventually, at the end of the stages, kriging map using anisotropic variogram was able to be developed with the smooth variant function of coordinate.

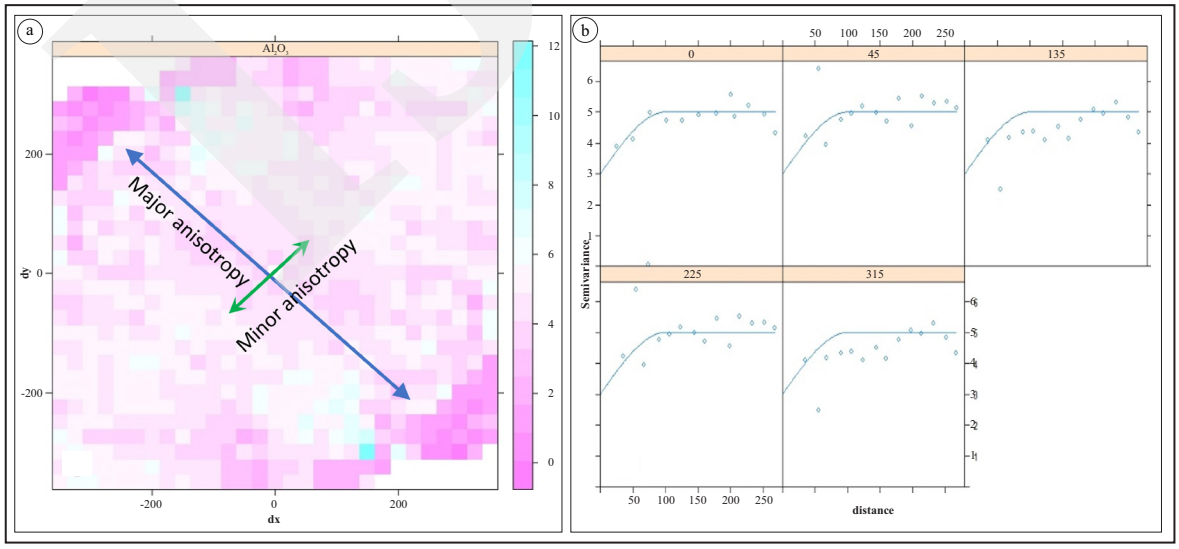

Figure 3. a) Variogram map of Al_2O_3 equipped with trend direction of anisotropy. b) Results of Al_2O_3 anisotropy variogram fitting grade using a spherical model in 0°, 45°, 135°, 225°, and 315° directions respectively.

Result and Analysis

Bauxite Weathering Profile

The vertical weathering profile of bauxite from top to bottom was observed from test pit and outcrops (Figure 4). The vertical profile comprises four horizons, such as latosol, bauxite, pallid/kong, and parent rock horizons. The physical properties of bauxite concretion size, weathering colour, and mineralogical characters are well preserved within test pit. In outcrop, these textures are sometimes disturbed by flowing of the rain-water which created furrow.

The exploration areas are situated in the tropical forest with massive vegetation cover. The root system facilitates drainage through rain-water percolation, enhances the leaching, and provides soluble organic compounds in the clayey soils of latosol zone. The more abundant content of organic compound leads to the precipitation of cation Fe^{3+} which causes the deep red to black colour. The thickness of this organic soil ranges from 0.5-2 m. The nature and thickness of latosol depend mainly on the parent rock texture, climate, the exposure of morphology, and groundwater circulation.

Bauxite horizon underlies the latosol and distinguished from the upper layer from the absence of root system and lesser accumulation of iron minerals. Heterogeneity of this layer is represented by the various textures, compositions, concretion size, and colour. The equidimensional textures are observed from the diverse shapes of nodules, concretions, and pisoliths which are embedded on the clay matrix. The size of concretion, nodule, and pisolith varies from 3.2-10 cm. In a test pit, from top to bottom, the bauxite size gradually changes to granule, and earthy ranging from 2 mm to 1.5 cm. This gradual changing apparently difficult to be observed in outcrop due to slope benching that overthrows the concretion downward. The colour vertically varies from orange, reddish-brown to brown. The total thickness of this horizon is approximately 0.8-6.8 m. Bauxite ore in the IUP Tayan was commercially classified as sponge ore or porous-textured bauxite.

Pallid/kong belongs to the saprolite horizon composed of predominant kaolinite as a weathering product of the parent rock. The accumulation of kaolinite occupies the upper part of kong, whilst to the bottom the mixed-layer structures of illite and montmorillonite may present. The

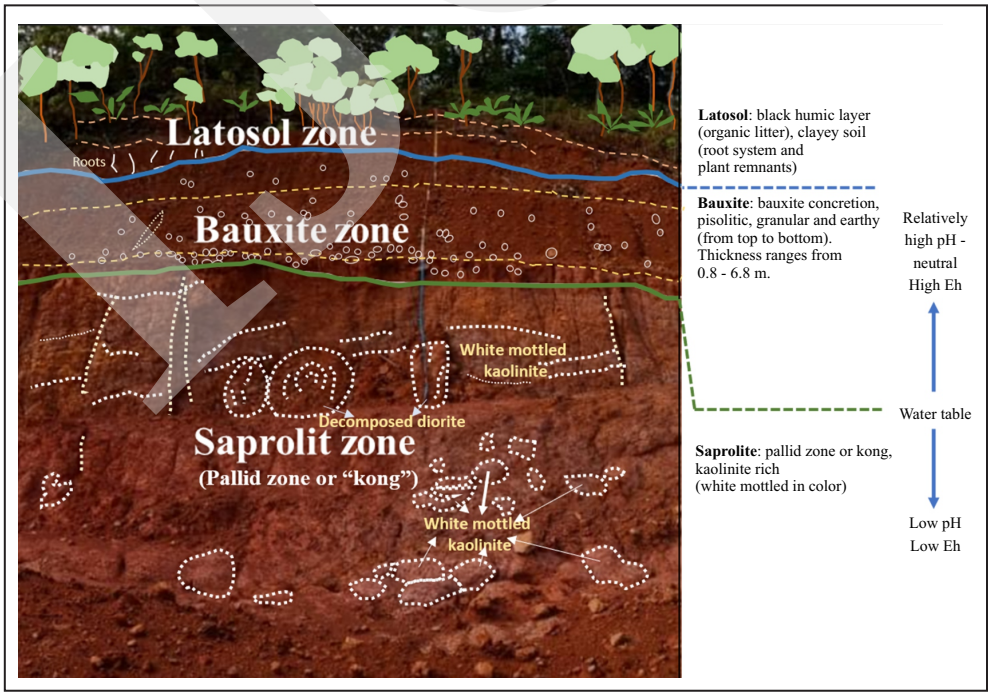

Figure 4. Outcrop photograph which is equipped with the sketch of a vertical weathering profile of bauxite.

saprolite has the lighter mottled colour of white kaolinite and greater thickness than the other two overlying horizons. Pitting is mostly terminated on the top horizon of pallid/kong since this horizon indicates the groundwater level. Thus, the whitish clay texture pronounced a degree of humidity (Sojien *et al*., 2018).

Parent rocks occupy the bottom part horizon and are rarely found from both test pits and outcrops. The identified source rock from local outcrop as diorite exhibits small parting (Figure 5a). Petrographically, diorite exhibits phaneritic, equigranular, holo-crystalline, composed of predominant plagioclase with lesser hornblende, quartz, alkali feldspar, and opaque minerals (Figure 5b). Sphene presents as an accessory mineral (Figure 5c), while mafic minerals partly altered to chlorite.

Bauxite Mineralogical Characteristics

Bauxite minerals are attributed to the element solubility of the primary minerals and the strength of the crystal lattice relative to weathering. The solubility is reliant on the internal rock properties, such as porosity, permeability, and grain size. However, the externally controlling variable of drainage and morphology affect the rate of mineral dissolution. Bauxite minerals are more likely precipitated in high Eh conditions which are situated several meters above the groundwater table.

According to the XRD and petrography observation, the main ore constituent of bauxite is gibbsite, while other neogenetic minerals may also present as assemblage minerals. Mineralogical composition and abundance of both bauxite and kong are compiled in Figure 6. From XRD analysis, the abundance of gibbsite corresponds to the equal proportion between silicate and iron-oxide minerals. A high percentage of either silicate or iron-oxide minerals is more likely to reduce the concentration of gibbsite. Sample of BX2 in Figure 6 conspicuously evidences the reduction of gibbsite content as silicate minerals present for about 40% of the total mineral composition. It indicates that bauxite zone experienced a frequent condition below groundwater level. In contrast, most of kong samples have abundant silicate minerals than gibbsite and iron-oxide minerals, revealing that this horizon is submerged below groundwater level.

The geometry of texture and mineralogical composition are well observed from petrography. Four major compositions of bauxite as observed using polarized microscope are gibbsite [iiγ-Al$(OH)_3$], iron minerals, clays, and quartz. Gibbsite presents as the most common alumina

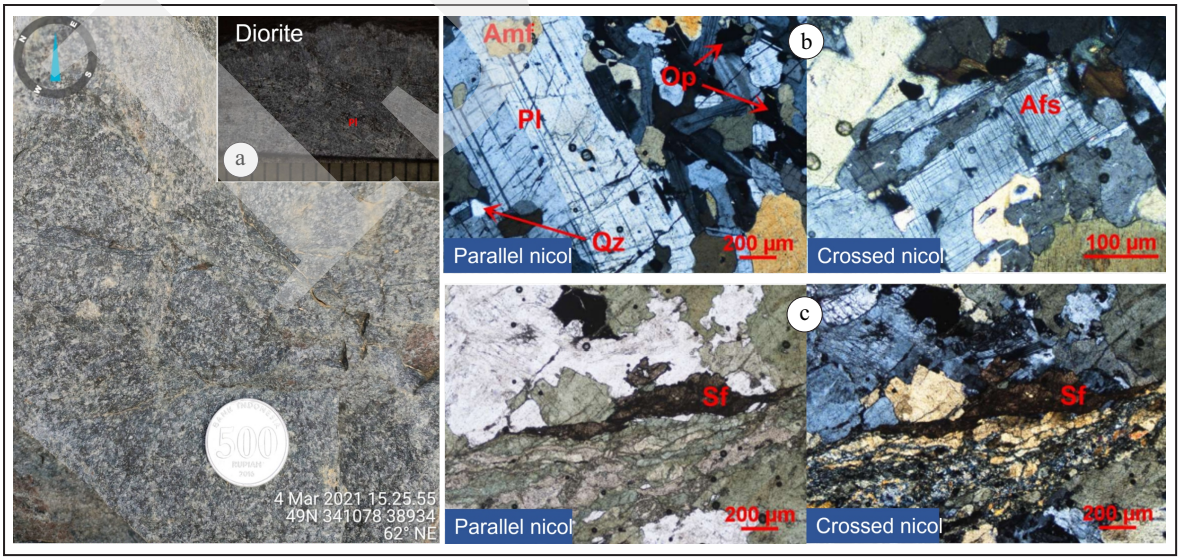

Figure 5. a) Hand specimen diorite; b & c) Parallel and crossed nicol light photomicrographs of diorite composed of plagioclase (Pl), amphibole (Am) as inclusion, alkali feldspar (Afs), quartz (Qz), and minor amount of sphene (Sf).

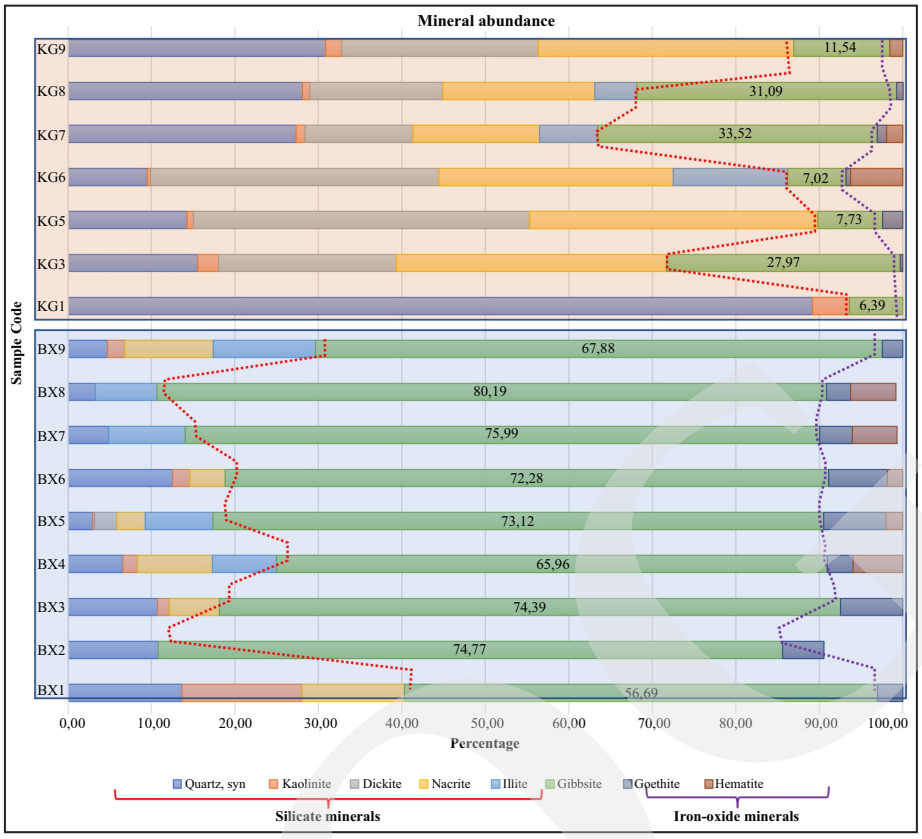

Figure 6. Mineralogical composition and abundance from XRD data.

mineral in abundance lateritic bauxites ranging from 6.39-80.19%. According to Nugraheni and Sunjaya (2019), the initial stage of mechanical weathering has evidenced by mineral cracking. The cracks were then enlarged with regards to groundwater penetration throughout the cracks. Gibbsite (Gbs) nucleation is suspected to occur mainly along the transmineral cracks of feldspar as the ultimate precipitation of kaolinite booklets (Figures 6, 7a and b). This mineral has been concentrated in the forms of nodules and concretions (Figure 7c), while in pisoids and ooids, gibbsite is concentrated in the matrix.

Iron minerals in hand specimen samples are frequently concentrated as goethite (α FeO(OH) and hematite (Fe_2O_3) with reddish-brown to brown colour. These minerals occasionally envelops the bauxite ore (Figures 6 and 7d) to form the rounded bauxite concretion. The XRD analysis denotes the ionic substitution of trivalent Al and V cations with the trivalent Fe in a goethite crystal lattice. Under the polarized microscope observation, these iron minerals present as opaque oxides (Ox-Fe in Figures 7a and b) that commonly associate with the fissures of primary minerals. Hematite co-exists with goethite and appears between relicts of primary mineral. Kaolinite as clay mineral is found intermixed with gibbsite and Fe-oxy-hydroxides (goethite) in bauxite horizon (Figures 7a dan b). Under the thin section observation of bauxite nodule, kaolinite exhibits in whitish pale colour which progressively takes place feldspar and subsequently altered to gibbsite. The photo-micrograph reveals the transition of kaolinite to gibbsite (Figures 7a and b Si-Gibs-Kln). Kaolinite predominates the clay constituent in kong/pallid horizon. The XRD examination facilitates the specific identification of kaolinite, dickite, and nacrite as well as other clay types of illite. Dickite and nacrite have the same composition as kaolinite but different in the crystal structure (polymorph). High content of silica has mainly accumulated in kong horizon rather than in bauxite. The increasing amount of dickite is equivalent to the amount

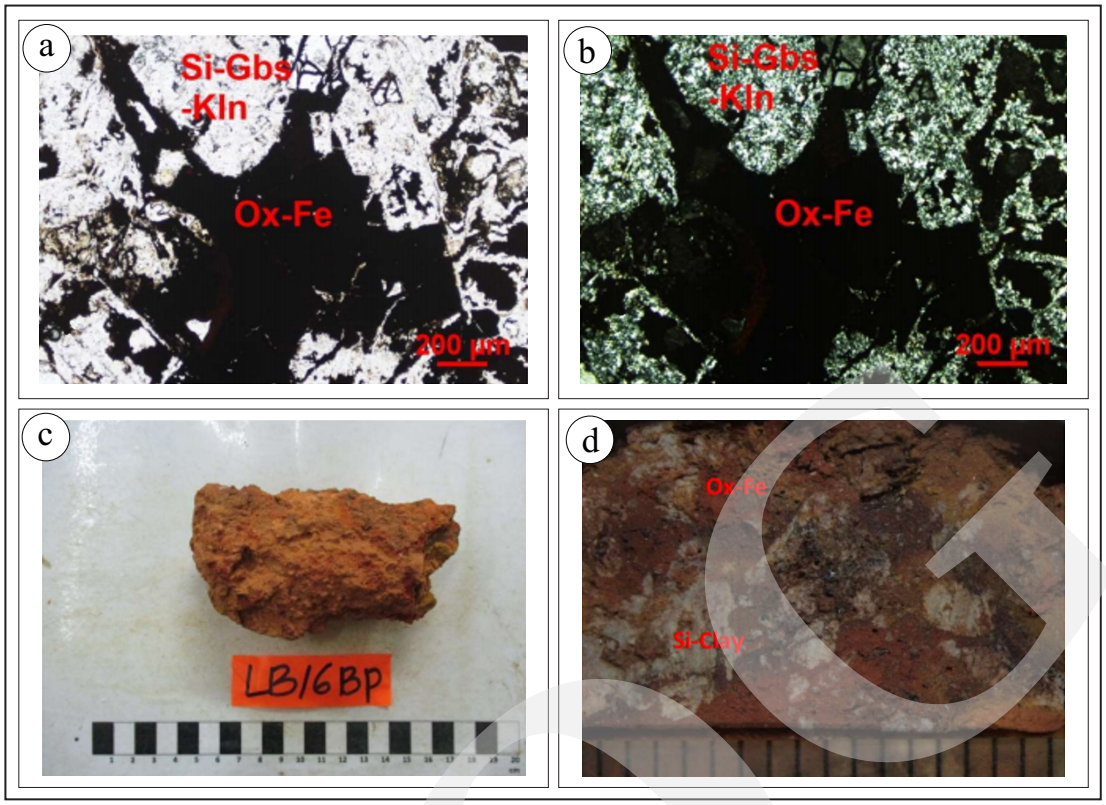

Figure 7. a and b) Photomicrographs of associate Fe-oxide and crypto-crystalline minerals (in the forms of silica, gibbsite, and kaolinite); c) Hand specimen sample of washed pisolith bauxite; d) Vertical slice sample of washed pisolith. (a. parallel nicols; b. crossed nicols).

of quartz. It is because dickite mineral is embedded in quartz minerals.

Index of Lateritization

About 296 bauxite samples analyzed using XRF have Total SiO_2 ($TSiO_2$) that ranges from 1.63 to 15.39 wt.%, reactive silica ($RSiO_2$) ranges from 0.56 to 4.63 wt.%, Al_2O_3 is recorded as 39.99 to 55.57 wt.%, Fe_2O_3 ranges from 6.99 to 29.06 wt.%, and TiO_2 from 0.17 to 3.2 wt.%. These data were then plotted to the ternary diagram of SiO_2-Fe_2O_3-Al_2O_3 to classify the mineralogical of bauxite ores (after Aleva, 1994). Plotting result shows that bauxite ores are mainly classified as

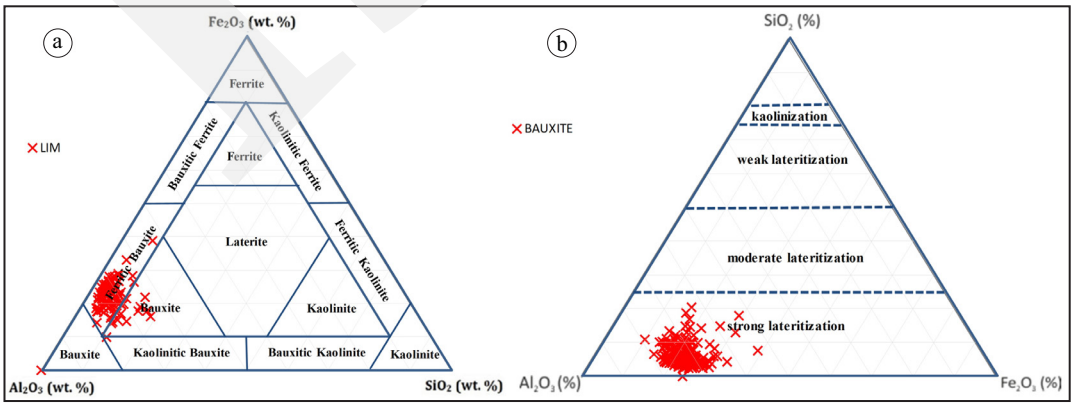

Figure 8. a) Ternary plot of Al_2O_3-Fe_2O_3-SiO_2 to classify the mineralogical classification of bauxite ores. b) Another plotting result of Al_2O_3-Fe_2O_3-SiO_2 in the ternary diagram of Schellmann (1981) showing degree of lateritization. Samples were distributed in a strong lateritization field or undergone bauxitization.

ferritic bauxite and bauxite (Figure 8a). In order to see the intensity of lateritization, the data has also been plotted to the second ternary of SiO_2-Fe_2O_3-Al_2O_3 as proposed by Schellmann (1981), while the index of lateritization (IOL) is determined using the following equation (Babechuk *et al*., 2014):

$$IOL = 100 \times \frac{(Al_2O_3 + Fe_2O_3)}{(SiO_2 + Al_2O_3 + Fe_2O_3)} \quad \text{..... (3)}$$

According to the ternary plot (Figure 8b), samples have undergone a strong lateritization to the peak of Al_2O_3 or specifically defined as bauxitized. Meanwhile, the IOL value illustrates a variation of laterite (average IOL: 81.29), lateritic bauxite (average IOL: 83.81 - 95.68), and bauxite (average value IOL: 95.70-97.29). The higher IOL value denotes higher content of Al_2O_3. Similarly, higher IOL value also represents excessive silica removal from weathering profile through intensive weathering and leaching process. In other words, it is defined as desilication. During bauxitization, deferruginization or releasing of iron element took place in the late stage of bauxitization (Figure 8b).

Result of Simulation

The initial result from R simulation is the kriging map. This map illustrates the predicted grades of each inputted elements. The predicted grades from the unexplored area are as follows: Al_2O_3 ranges from 47.08 wt.% to 53.55 wt.% (Figure 9), Fe_2O_3 ranges from 11.91 wt.% to 18.85 wt.%, the total silica ($TSiO_2$) ranges from 2.00 wt.% to 10.84 wt.%, and reactive silica ($RSiO_2$) ranges from 0.67 wt.% to 2.82 wt.%. The predicted value needs to verify using cross-validation, but prior to the validation check, kriging variance may also essential to identify the difference between the predicted and actual value.

The greater distances from available test pit data lead to greater variance value. The predicted value in the predicted area -2, which is situating

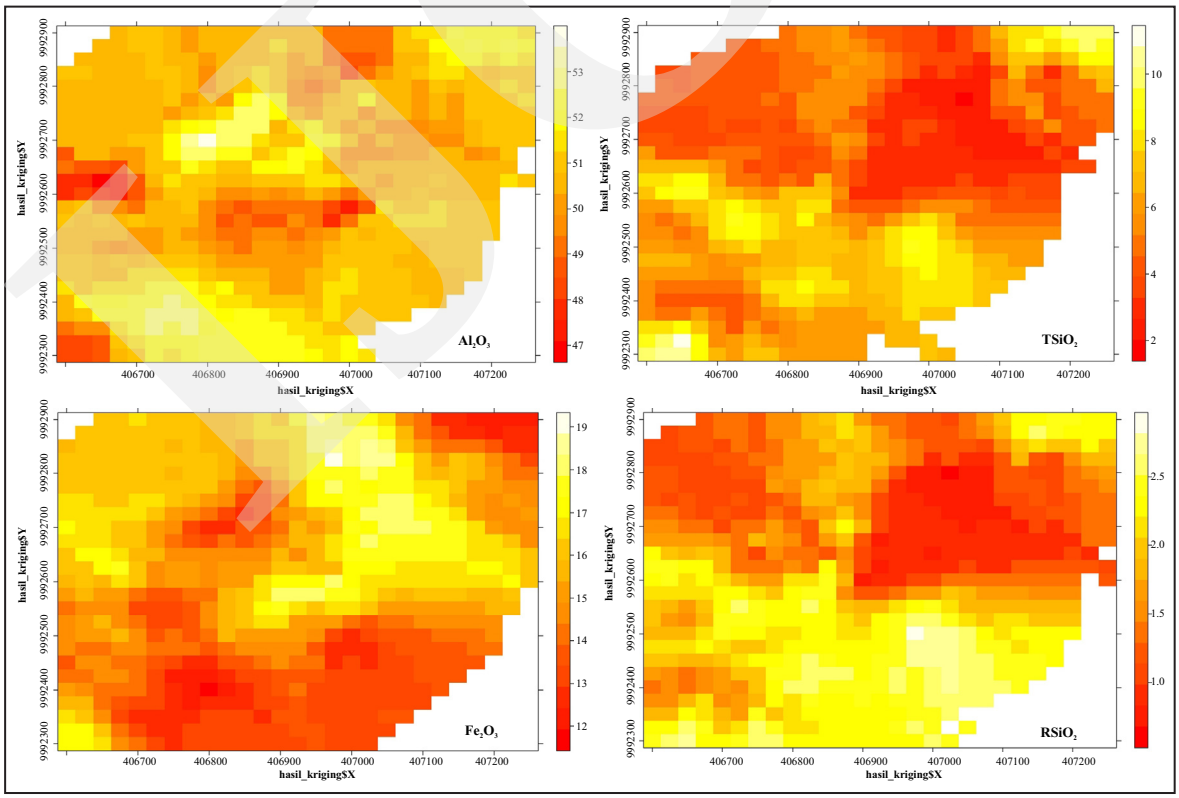

Figure 9. Predicted and observed value of Al_2O_3, $TSiO_2$, Fe_2O_3 and $RSiO_2$ from ordinary kriging as simulated using R.

in between the available test pit data, has a lesser variance value than the predicted area -1 with none of the adjacent data.

(Figure 10). Thus, the massive data will strengthen the grade extrapolation.

The following stages are cross validation, where the summary of cross validation for each observed element is tabulated in Table 1 and Figure 11. In Figure 11, the correct predicted value should be along the line. Overall, a negligible error was found for kriging simulation. Despite the negative ME value for Al_2O_3 and Fe_2O_3, their values are still close to 0, and there is a hope to gain a slightly higher grade during the following exploration.

Different from kriging that utilizes variogram to do estimation and produces smooth extrapolation, simulation illustrates different map results but relatively similar pattern one to another or termed as an equiprobable image. The simulation represents a true condition than kriging maps. Orebody estimation using kriging is difficult to see the uncertainty of the results as it has a single response. In the meantime, simulation has a distribution curve as multiple responses. R data analysis is able to generate several simulation results as depicted in Figure 12. From ten simulations, the representative grade distribution has to be carefully selected by considering the geological condition of the studied area, such as morphology, groundwater level, types of parent rock, and many more. Simulation 7 closely represents the geological condition in the studied area.

Discussion

Grade Extrapolation *vs.* IOL

With regards to the internal and external controlling variables of bauxite formation, the increasing grades of aluminium and decreasing content of silicate and iron minerals rely mainly on the rising rates of rainfall to increase the water percolation. The enrichment is also governed by the direction of groundwater fluctuation through the slope of topography and the degree of dehydration during dry seasons. From the reconstruction of universal kriging in Figure 13, it is noticed that the estimated area in the centre of the UK map has the best ore grade quality as evidenced by the higher ore grade of Al_2O_3 (52.00 wt.% - 53.29 wt.%) with a low grade of $TSiO_2$ (2.09 wt.% - 6.10 wt.%), $RSiO_2$ (1.00 wt.% - 2.31 wt.%), and Fe_2O_3. The predicted grades of Al_2O_3

Table 1. Results of Cross-validation Method from Predicted Grades of Al_2O_3, Fe_2O_3, $TSiO_2$, and $RSiO_2$ in wt.% Unit

Major Elements	ME	MSDR
Al_2O_3	-0.033	0.9724
Fe_2O_3	-0.023	0.9956
$TSiO_2$	0.063	1.0047
$RSiO_2$	0.012	0.9340

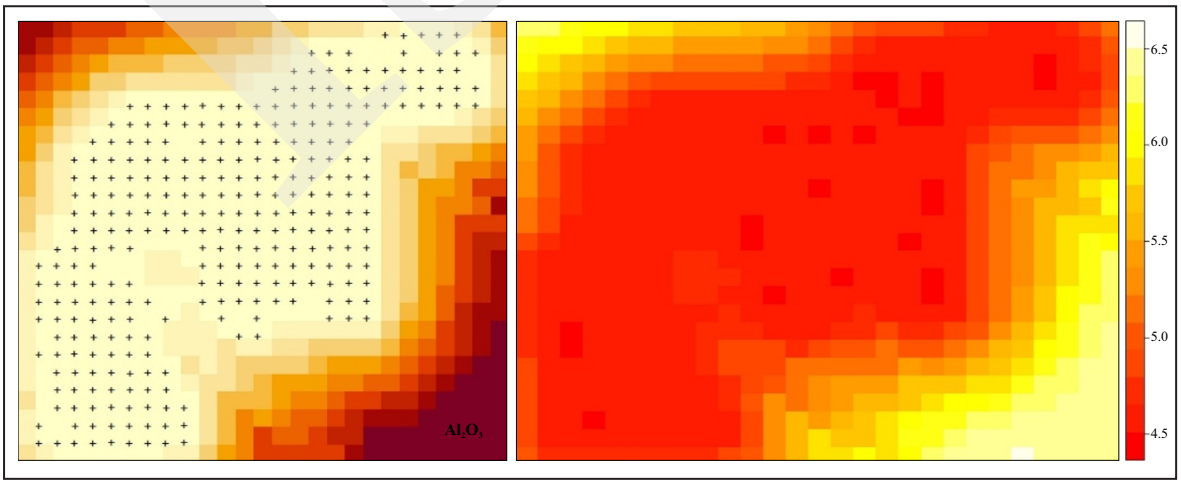

Figure 10. Two types of kriging variance for Al_2O_3 as simulated using R data analysis.

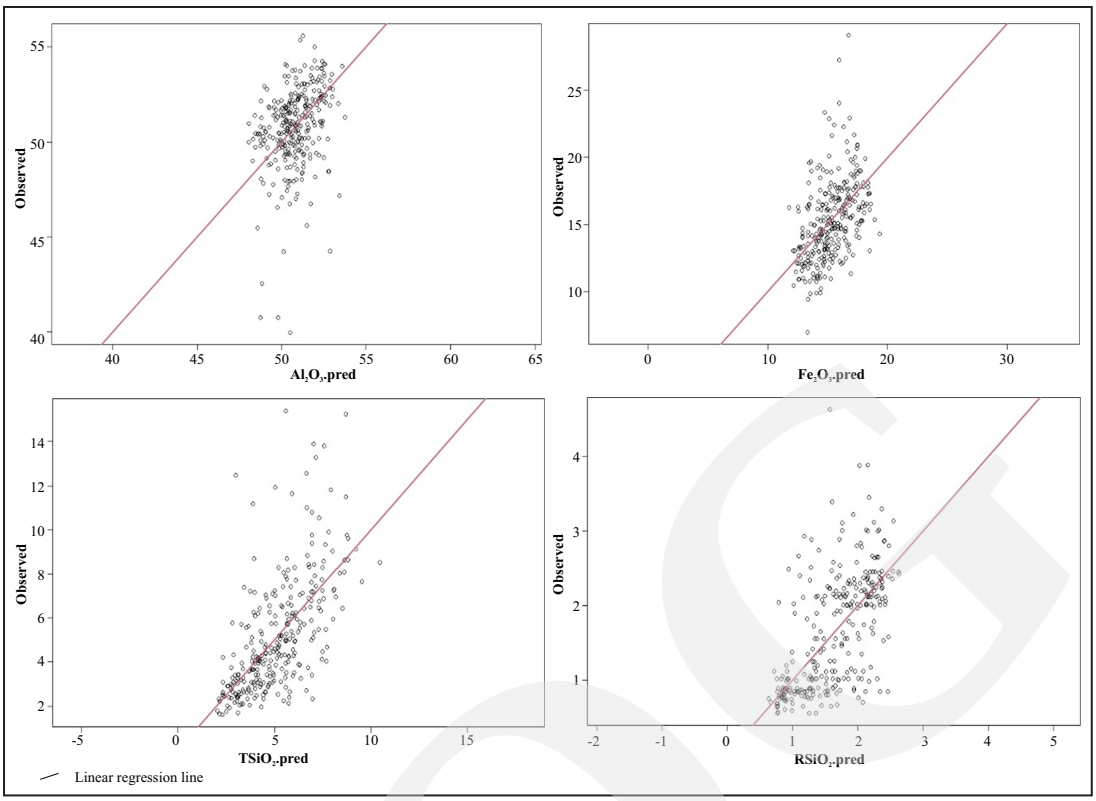

Figure 11. Cross-validation result is estimated according to the deviation of the predicted value as indicated by dots surrounding the red line.

Figure 12. Ten simulation results (right) as equiprobable image.

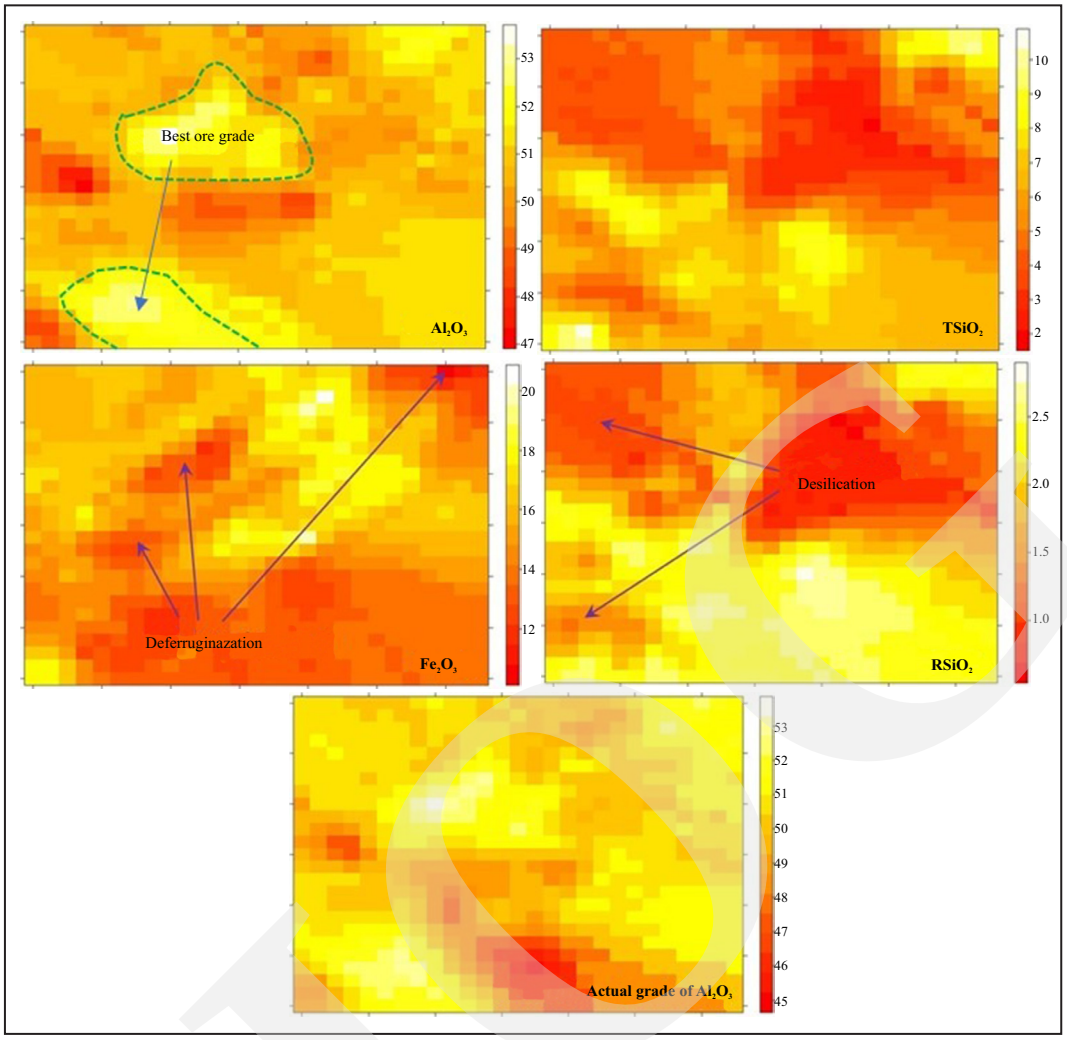

Figure 13. a) Maps of Universal Kriging (UK) using anisotropic variogram. The upper four maps are kriging estimation for Al_2O_3, Fe_2O_3, $TSiO_2$, and $RSiO_2$, while the bottom map is the actual grade distribution of Al_2O_3.

in the southwest direction (predicted area -2) have a similar content of alumina, but contains slightly high grades of $RSiO_2$. However, it should be noted that despite bauxite samples underwent washing treatment, the observed element content is envisaged as in natural condition, since consistent beneficiation process was applied during sample preparation.

Mineralogical distribution proves that the abundant gibbsite with a minor content of iron oxide and kaolinite minerals are subjected to the high grade UK map of Al_2O_3. The mineral abundance in this area is gibbsite that ranges from 65.96 to 80.19%, followed by a minor amount of iron oxide minerals which are present in the forms of hematite (1.87 - 5.96%) and goethite (2.88 - 7.48%) as well as kaolinite (0.19 - 2.07%). It can be assumed that the best ore grade occurred in conjunction with groundwater fluctuation, in which desilication took place under reduction condition once the weathered rock submerged below the groundwater level. During this time, extensive leaching occurred as evidenced by the high silica removal. Meanwhile, once the weathered rock is exposed to the surface, deferrunization takes place under oxidation condition to alter ferruginous minerals (amphibole and pyroxene) into hematite and goethite.

The estimated grade value that lies in the northwest (predicted area -1) and southeast, commonly has low grades of bauxite ore. This is because they have either greater grades of

Fe_2O_3, $TSiO_2$, or $RSiO_2$ as a function of different response toward local physiochemical weathering environments and topography. This assumption is supported by the trend of major anisotropy in variogram map that extent in NW - SE direction. The northeast direction is considered to be a high silica bauxite area which is suspected to form near the surface of groundwater level. The interpretation is also evidenced by the existence of a river in the proximity of the weathering profile.

Comparison of IOL kriging map with Al_2O_3 using 10 m grid distance reveals that the predicted areas in the south-southeast and northwest directions have a positive correlation of lateritic bauxite (Figure 14). The IOL value in the predicted areas is 91-94, while the grade of Al_2O_3 ranges from 49 wt.% to 51wt.%. Nonetheless, a high value of IOL in the west direction exhibits lower grades of Al_2O_3 <49 wt.% as denoted with red grade colour (Figure 14b). It is suggested that the area experienced extreme alteration during upward drainage, so both iron and silicate minerals exist.

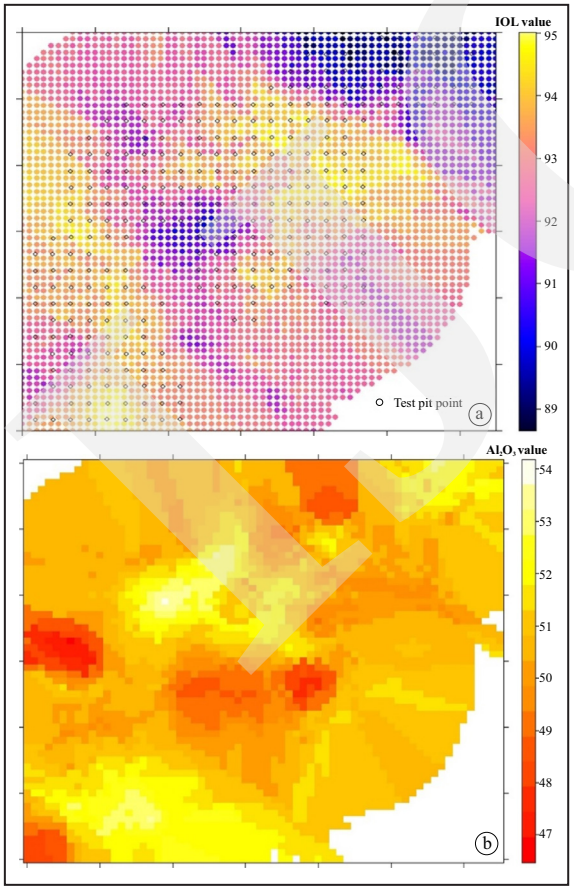

Figure 14. a) Kriging map of Index of Lateritization (IOL) and b) Kriging estimation for Al_2O_3 grade. Grid point was set up for 10 m.

Conclusions

The vertical weathering profile of bauxite demonstrates intense weathering under seasonal warm-humid climate. The weathering profile of the studied laterite in Tayan District is produced from the weathering of diorite rocks. Bauxitization generates gibbsite mineral as a major component of bauxite ore. Higher content of bauxite ore or best ore grade in the predicted areas presents in correspond to the excessive silica and iron removal (desilication and deferruginization) due to leaching in the late stage of bauxitisation. The enrichment of Al_2O_3 content is suggestive of the natural occurrence of kaolinite breakdown under reduction condition. As groundwater fluctuated, under oxidizing conditions, dehydration took place along with the formation of Fe-oxide minerals in the forms of hematite and goethite. These minerals sufficiently preserved bauxite ore, although a higher grade of Fe-oxide minerals will reduce the grade of Al_2O_3 as evidenced in Figure 13. Both pH and redox condition contribute to the bauxite formation and grade enrichment.

The volume of the water table is reliant on the rainfall water percolation that decreases pH value. The acidity suggests that groundwater mainly contains soluble CO_2 with lesser SO_2 and NO_2. Accordingly, the increasing rate of rainfall has contributed to strong lateritization. Nonetheless, the climate is not the only factor that governs the enrichment of Al_2O_3. Its enrichment was also controlled by the fluctuation of groundwater level with regards to the topography condition. Low topography areas, in the vicinity of intermittent stream or swamp, experienced intense leaching under reduction condition as evidenced by the high content of $RSiO_2$ and $TSiO_2$ with lesser content of Fe_2O_3 in the predicted areas.

Thanks to R for facilitating the ore grade interpolation with a quick and reliable result. The platform has flexibility in adjusting result as it was also equipped with statistical cross-validation to ensure the simulation quality. The accuracy of predicted ore grade value was assessed by comparing the actual data from the latest exploration with the predicted results from R simulation. Negative Mean Error (ME) was used as a cross validation to determine the degree of bias during estimation. Overall, the value of ME is close to zero or has a negligible bias prediction. The negative ME value was observed for Al_2O_3 and Fe_2O_3, suggesting the predicted grade was lower than the actual value. As the spatial simulation model is presented in a pixelated picture format, a closer grid set up, and massive data is able to disguise the appearance. The grade distribution from this model assists the explorationist to locate good quality resources from the available data.

Acknowledgments

The authors would like to express the greatest thanks to Unit Geomin P.T. Antam, Tbk. for giving a valuable access to geochemical data to finalize this research study by implementing a statistical concept for data extrapolation.

References

Aleva, G.J.J., 1994. *Laterites: Concepts, Geology, Morphology and Chemistry*. International Soil Reference and Information Centre (ISRIC), Wageningen, The Netherlands, 169pp. DOI: 10.1180/claymin.1996.031.3.15.

Babechuk, M.G., Widdowson, M., and Kamber, B.S., 2014. Quantifying chemical weathering intensity and trace element release from two contrasting basalt profiles, Deccan Traps, India. *Chemical Geology*, 363 (7), p.56-75. DOI: 10.1016/j.chemgeo.2013.10.027.

Bivand, R.S., Pebesma, and E.J., Rubio, V.G., 2008. *Applied Spatial Data Analysis with R, Human Immunology*. Springer Science+Business Media, LLC, New York. DOI: 10.1016/j.humimm.2007.08.003.

de Smet, M.E.M. and Barber, A.J., 2005. Tertiary stratigraphy. *In*:Barber, A.J., Crow, M.J., and Milson, J.S. (eds.), Sumatra: Geology, Resources, and Tectonic Evolution. *Geological Society Memoir*. DOI: 10.1144/GSL.MEM.2005.031.01.07.

Hall, R., 2002. Cenozoic geological and plate tectonic evolution of SE Asia and the SW Pacific: Computer - based reconstructions, model, and animations. *Journal of Asian Earth Sciences,* 20 (4), p.353-431. DOI: 10.106/S1367-9120(01)00069-4

Hall, R., 2018. *Sundaland: basement character, structure and plate tectonic develoment*, DOI: 10.29118/ipa.2374.09.g.134.

Hedenquist, J.W., Thompson, J.F.H., Goldfarb, R.J., Richards, J.P., Freyssinet, P., Butt, C.R.M., Morris, R.C., and Piantone, P., 2019. Ore-Forming Processes Related to Lateritic Weathering. *In*: *One Hundredth Anniversary Volume*. DOI: 10.5382/av100.21.

Herrington, R., Mondillo, N., Boni, M., Thorne, R., and Tavlan, M., 2016. Chapter 14 Bauxite and Nickel-Cobalt Lateritic Deposits of the Tethyan Belt. *Economic Geology, Special Publication*.

Kabacoff, R.I., 2011. R IN ACTION: Data analysis and graphics with R, Online. DOI: 10054678.

Metcalfe, I., 2011. Tectonic framework and Phanerozoic evolution of Sundaland. *Gondwana Research,* 19 (1). p. 3-21. DOI: 10.1016/j.gr.2010.02.016.

Metcalfe, I., 2017. Tectonic evolution of Sundaland. *Bulletin of the Geological Society of Malaysia*, 63, p.27-60. DOI: 10.7186/bgsm63201702.

Nugraheni, R.D. and Sunjaya, D., 2019. Geochemical Approach to Reveal the Genetic Occurrence of Gibbsite, Relative to the Parent Rock Type in Lateritic Bauxites. *Journal of Physics: Conference Series,* 1363, 012042. DOI: 10.1088/1742-6596/1363/1/012042.

Oriani, F., Straubhaar, J., Renard, P., and Mariethoz, G., 2014. Simulation of rainfall time series from different climatic regions using the direct sampling technique. *Hydrology and Earth System Sciences,* 18 (8), p. 3015-3031. DOI: 10.5194/hess-18-3015-2014.

Pirot, G., Straubhaar, J., and Renard, P., 2014. Simulation of braided river elevation model time series with multiple-point statistics. *Geomorphology,* 214, p.148-156. DOI: 10.1016/j.geomorph.2014.01.022.

Putzolu, F., Papa, A.P., Mondillo, N., Boni, M., Balassone, G., and Mormone, A., 2018. Geochemical characterization of bauxite deposits from the Abruzzi Mining district (Italy). *Minerals*, 8 (7), 25pp. DOI: 10.3390/min8070298.

Schellmann, W., 1981. Considerations on the definition and classification of laterites. *Proceedings of international seminar on* Lateritisation processes, IGCP 129 and IAGC, *Trivandrum, India*. Oxford and IBH Publishing Company, New Delhi, p.1-10. DOI: 10.1016/0341-8162(94)90007-8.

Schellmann, W., 1986. A new definition of laterite. *Memoirs of the Geological Survey of India*, 120, p.1-7.

Sojien, T.M., Mamdem, E.L.T., Wouatong, A.S.L., and Bitom, D.L., 2018. Mineralogical, Geochemical and Distribution Study of Bauxites in the Locality of Bangam and Environs (West Cameroon). *Earth Science Research*, 7 (1), p.117-140. DOI: 10.5539/esr.v7n1p117.

Song, Y.C., Liu, Z.N., Meng, H.D., and Yu, X.Y., 2019. Multi-point geostatistics for ore grade estimation. *Geologia Croatica,* 72, p.111-126. DOI: 10.4154/gc.2019.23.

Strebelle, S., 2002. Conditional simulation of complex geological structures using multiple-point statistics. *Mathematical Geology*, 34, p.1-21. DOI: 10.1023/A:1014009426274.